RSC Advances

PAPER

View Article Online
View Journal | View Issue

Cite this: *RSC Adv.*, 2024, **14**, 15647

Synthesis of phenol formaldehyde resin (PFR) based fluorescence resonance energy transfer (FRET) composites for double channel detection of latent fingerprints

Ping Yang, * Tingfei Shi, Zhiyuan Liu, Siying Wu, Yuqi Cheng, Kuiliang Li and Hong Zhao

A reversible two-channel fluorescent nanocomposite with fluorescence resonance energy transfer (FRET) effect was designed for the development, analysis, and characterization of latent fingerprints (LFPs). For the construction of the FRET probe, a core of mesoporous silicas (MSNs) were used to encapsulate the organic dye rhodamine 6G (RhD-6) as an acceptor, while green-emitting monodisperse phenolic resin nanoparticles (PFR NPs) were selected as a donor. The up-conversion material (UC) of $NaYF_4$:Yb,Er was synthesized using a simple hydrothermal method, and the MSNs-RhD-6/PFR (PRM) was electrostatically adsorbed onto the UC nanoparticles using a layer-by-layer method to obtain MSNs-RhD-6/PFR-UC (PMU). Compared to ordinary single-channel materials, PMU can be excited by different light sources (365 nm UV/980 nm laser) and its fluorescence can be reversibly switched between yellow and green, demonstrating excellent light reversibility. The PMU composites were successfully used to visualize and detect LFPs on various substrate surfaces using a simple powder coating method. Due to the existing FRET effect and dual-channel characteristics, this composite material displays excellent contrast, outperforming commercially available products for wider applicability. Even on complex backgrounds and after aging or washing treatments, it still clearly recognizes fingerprints in first-, second-, and third-level details, showing its great potential in latent fingerprint detection.

Received 1st March 2024
Accepted 1st May 2024

DOI: 10.1039/d4ra01613k

rsc.li/rsc-advances

1. Introduction

Fingerprints have long been recognized as the most reliable form of identification due to their unique and unchanging nature. Each individual's fingerprints possess distinctive characteristics that remain constant throughout their lifetime, making them an invaluable tool in criminal investigations.[1–4] Latent fingerprints (LFPs) are often difficult to detect without specialized visualization methods due to their invisibility to the naked eye.[5,6] The visualization of LFPs on complex surfaces remains a significant challenge, with powder dust removal and chemical treatment methods being the most commonly utilized techniques among various reported methods. Conventional powders mainly have certain drawbacks, including toxicity, low contrast, high background interference, and low selectivity.[7–10] Although chemical methods like iodine fumigation,[11] ninhydrin,[12] and silver nitrate have seen rapid development in recent years,[13] they still have some disadvantages, such as slow reaction speed, background reaction, and potentially destructive effects on fingerprints.[8,14] These limitations greatly restrict the applicability of current materials in fingerprint visualization. To address these issues, urgent development of nanomaterials with high sensitivity, resistance to background interference, strong fluorescence emission, and excellent adsorption properties is necessary in the field of criminal investigation.

In recent years, there has been rapid development in upconversion material nanoparticles (UC NPs), particularly for LEP detection in the optical field. UC NPs, unlike conventional down-conversion fluorescent materials, exhibit an anti-Stokes shift feature, emitting shorter wavelength luminescence upon excitation with longer wavelengths. Handprints with UC NPs have been shown to produce minimal background fluorescence, resulting in improved optical contrast and higher detection sensitivity.[15,16] A recent study by Wang *et al.* explored a handprint assay that integrated nanoscale UC NPs with lysozyme-binding aptamers, showcasing the potential of UC fluorescence to mask the background fluorescence of the substrate.[17] $NaYF_4$ crystals with low vibrational energy (<400 cm^{-1}), low non-radiative attenuation rate and high radiative emissivity have become a new focus of research, especially for Yb^{3+}/Er^{3+} and Yb^{3+}/Tm^{3+} up-conversion systems.[18–21] Baride group combined β-$NaYF_4$:2%Tm with $NaYF_4$:48%Yb to form a near-infrared (NIR) UC NPs system for latent fingerprint

School of Chemical Engineering, Anhui University of Science and Technology, Huainan, Anhui, 232001, P. R. China. E-mail: pyang8066@163.com

detection.[22] SiO_2 nanomaterials have been studied for their unique structure, good photophysical properties and easy surface functionalization modifications.[8,23,24] They are used in large quantities to form novel materials with different functional materials in composite for specific functions. Coating fluorescence material into MSN could keep the good adhesive and low toxicity due to the good biocompatibility of MSN through the fluorescence partly decrease.[23,25] Wang's group synthesized silica-coated $NaYF_4$ up-conversion nanomaterials ($NaYF_4$@SiO_2) by controlling the ratio of nanorods to silica.[26] These up-conversion nanomaterials exhibit different morphologies of nano-dumbbells and nanowires with higher fluorescence efficiency and have enormous potential in forensic science.

To improve the contrast and sensitivity of fluorescent probes, fluorescence resonance energy transfer (FRET) has been widely used as a very effective means in the field of chemical analysis and chemical sensors. In recent years, this course group has synthesized monodisperse phenolic resin (PFR) NPs with green luminescence using a simple one-step hydrothermal method.[27,28] The synthesized PFR NPs have a significantly broad emission band at 536 nm, which makes them energy donors in FRET systems.[29]

Herein, rhodamine 6G (RhD-6) embedded into mesoporous silica (MSNs) yielded MSNs-RhD-6 nanospheres as acceptors, which are optimally excited near 528 nm, where their emission and absorption bands mostly overlap. Therefore, a novel FRET nanocomposite MSNs-RhD-6/PFR (PRM) was obtained by electrostatic adsorption of PFR NPs and MSNs-RhD-6. Further, we fabricated a reversible dual-channel fluorescent material, MSNs-RhD-6/PFR-UC (PMU), by combining a $NaYF_4$:Yb,Er (UC) material with upconversion properties with a PRM with FRET effect. This material is capable of reversibly switching between yellow and green fluorescence under 365 nm UV or 980 nm laser excitation, which significantly improves sensitivity, resistance to background interference and detection accuracy.

2. Experimental

2.1 Materials and chemicals

Yttrium(III) oxide(Y_2O_3), Ytterbium(III) oxide(Yb_2O_3), Erbium(III) oxide(Er_2O_3), 3-aminopropyltriethoxysilane (APTES), Poly(4-styrene sulfonate) sodium (PSS), Polyethyleneimine (PEI), Rhodamine 6G(RhD-6) *P*-Chlorophenol and Oleic acid (OA) were purchased from Shanghai Aladdin Reagent Co. Cetyltrimethylammonium bromide (CTAB), Tetraethyl orthosilicate (TEOS), Triethanolamine (TEA), Sodium hydroxide, Sodium fluoride, Calcium cyclic carbonate, Cyclohexane, Anhydrous ethanol, Hexamethylenetetramine(HMT) and Hydrochloric acid were provided by Sinopharm Chemical Reagent Co. All chemicals were used as analytical grade without further purification.

2.2 Synthesis of UC nanoparticles

Put 2.8226 g of Y_2O_3, 1.7454 g of Yb_2O_3, and 0.4782 g of Er_2O_3 into a round bottom flask with 10 mL of concentrated hydrochloric acid and 10 mL of deionized water, respectively, and stir at reflux in an oil bath at 58 °C until completely dissolved, after dissolution, the oil bath was heated up to 120 °C to evaporate and dry the solvent. The UC material was synthesized according to the reported literature with little modification. The evaporated product was prepared by adding a small amount of deionized water to prepare the rare earth salt, and then fixed with a 50 mL volumetric flask and set aside. The NaOH solution and NaF solution were prepared by adding 1 g of NaOH to 5 mL of deionized water and 0.4175 g of NaF to 5 mL of deionized water and set aside.

1 mL of YCl_3 solution, 0.9 mL of $YbCl_3$ solution and 0.4 mL of $ErCl_3$ solution were added to a mixture of 0.3 mL of NaOH solution, 5.0 mL of OA and 10.0 mL of ethanol, respectively, and 3 mL of NaF solution was added drop by drop to the above mixture and stirred for 30 minutes to form a colloidal solution. Then, the colloidal solution was transferred to a 30.0 mL PTFE-lined autoclave heated at 200 °C for 10 hours. The solution was cooled naturally and washed several times by centrifugation with a 1 : 1 mixture of ethanol and cyclohexane. Finally, the product was placed in a vacuum at 60 °C to obtain a dry powder for further application.

2.3 Synthesis of PFR

The synthesis of chlorine-containing phenolic resin (Cl-PFR) nanomaterials was optimized using the method with some modification, according to the method reported previously by our group.[30] A mixture of 0.0841 g of HMT and 0.0257 g of *p*-chlorophenol was dissolved in 30 mL of deionized water under magnetic stirring. Then, the mixture was subjected to a hydrothermal reaction at 160 °C for 5 hours. Subsequently, the resulting product was collected with centrifugation and washed with deionized water several times.

2.4 Synthesis of RPM

Highly dispersed mesoporous silicas (MSNs) with uniform particle size were synthesized following a modified method proposed by Bein *et al.* with little modification.[31] Specifically, a solution containing RhD-6 (8 mg), CTAB (0.5 g), and TEA (80 mg) in 20 mL of deionized water was stirred at 90 °C for 6 h. Subsequently, 3 mL of TEOS was added dropwise and the stirring continued for another 3 h. The resulting SiO_2-RhD-6 nanospheres were obtained after drying in a vacuum for 12 h. This powder was then mixed with 40 mL of ethanol and the pH was adjusted to 4 using hydrochloric acid. The mixture was heated to 76 °C and refluxed for 3 h. After washing the powder with ethanol three times, it was dried in a vacuum for 12 h. Subsequently, the powder was treated with 1 mL of APTES in 40 mL of ethanol, followed by refluxing with stirring for 6 hours. Excess APTES was removed by washing with ethanol and the resulting aminocarbamoylated MSNs-RhD-6 powder was dried in a vacuum oven. The resulting precipitate was collected for the synthesis the produce of PFR/MSNs-RhD-6 (RPM).

2.5 Synthesis of PMU

Through alternately adsorbing poly(sodium 4-styrene sulfonate) (PSS) and polyethyleneimine (PEI) onto the surface of UC

nanoparticles using the layer-by-layer method, the polyelectrolyte (PSS/PEI/PSS) was synthesized. Then 8 mg of UC decorated with polyelectrolyte and 20 mg of RPM [$m(UC^{-}) : m(PRM) = 5 : 2$] were added to 20 mL of deionized water, stirred thoroughly and left to stand in a dark environment for 4 hours. Then, the precipitate was collected by centrifugation at 10 000 rpm for 5 minutes, washed with deionized water and ethanol three times, and finally dried under vacuum for 24 hours to obtain PMU powder.

2.6 Characterize

Qiwei WFH-204B UV analyzer provides 365 nm UV light. The 980 nm laser light source is a homemade laser emission, power 5 W, through the homogenizer to expand the light spot. Photoluminescence (PL) spectra were obtained on a Cary Eclipse FL1011M003 (Varian) fluorescence spectrometer. The morphology of PMU was characterized using transmission electron microscopy (TEM, JEOL 2010F). X-ray diffraction (XRD, Cu Kα = 1.5418 A radiation) was performed on a PANalytical X 'Pert instrument. Fingerprint images were taken using a Sony a6000 with a 56 mm lens. Fingerprint details were analyzed using ImageJ, a free software developed by the National Institutes of Health.

3. Results and discussion

3.1 Synthesis and characterization of the FRET composites

As shown in Scheme 1, the PMU composites were prepared with three steps. Firstly, the RhD-6 was embedded into MSNs in the synthesis process. After decorating PFR NPs into MSNs-RhD-6 to obtain the RPM, the amine group was further modified on the surface of MSNs with APTES to increase the positive electricity of the RPM nanosphere. Secondly, as shown in Scheme 1b, the up-conversion UC was prepared with the hydrothermal method. Finally, the polymer of PSS and PEI modified UC nanoparticles were mixed with the positive electrode PMU to form the RPM composites. Due to the excellent fluorescence of RPM and UC under UV/IR irradiation, the good adhesion of MSNs and the positive charge of NH_2 and LFP on different surfaces was detected by the powder coating method sensitively. Furthermore, the MSNs can be absorbed by the LFPs strongly due to the modified amine group, which can strongly affect the amino acid in LFPs.

The crystalline phase and composition of the prepared materials were analyzed using XRD. In Fig. 1, line a shows a slight broad peak band near 23°, which easily corresponds to the broad peak located at 22.8° of SiO_2. In line b, the peaks located at 17.14, 29.96, 30.81, 34.74, 39.67, 43.47, 46.51, 52.07, 53.17, 53.72, 55.26, 61.25, 62.26, 64.13, 65.08, 71.03, 72.35 and 77.62 correspond to the peaks of UC (PDF#28-1192) of (100), (110), (101), (200), (111), (201), (210), (002), (300), (211), (102), (112), (220), (202), (310), (311), (212), and (302) crystalline phases, and peaks at 28.22° correspond to (111) crystal plane of $NaYF_4$ (PDF#77-2042). The results indicate that the synthesis of PMU composites was successfully prepared.

Fig. 2a shows the FTIR spectra of the Cl-PFR nanoparticles. The presence of C=O and hydroxyl functional groups is known from the characteristic absorption peaks at 3423 and 1636 cm^{-1}. The C=C stretching IR absorption peak on the benzene ring is at 1476 and the peak at 1220 cm^{-1} corresponds to the C–H in-plane bending vibration peak on the benzene ring. In addition, the absorption peaks at 1271 and 1116 cm^{-1} are attributed to the C–Cl and C–C stretching vibrations, and the in-plane deformation peak position of the H–H stretching coupling occurs at 818 cm^{-1}. Thus, it is proved that the synthesis of Cl-PFR, as well as the products, contain the presence of Cl elements. Fig. 2b shows the FTIR spectra of PRM and PUM composites. The presence of strong absorption peaks of PRM around 3438 and 1638 cm^{-1} can be observed in line a, which is attributed to the stretching vibration and bending

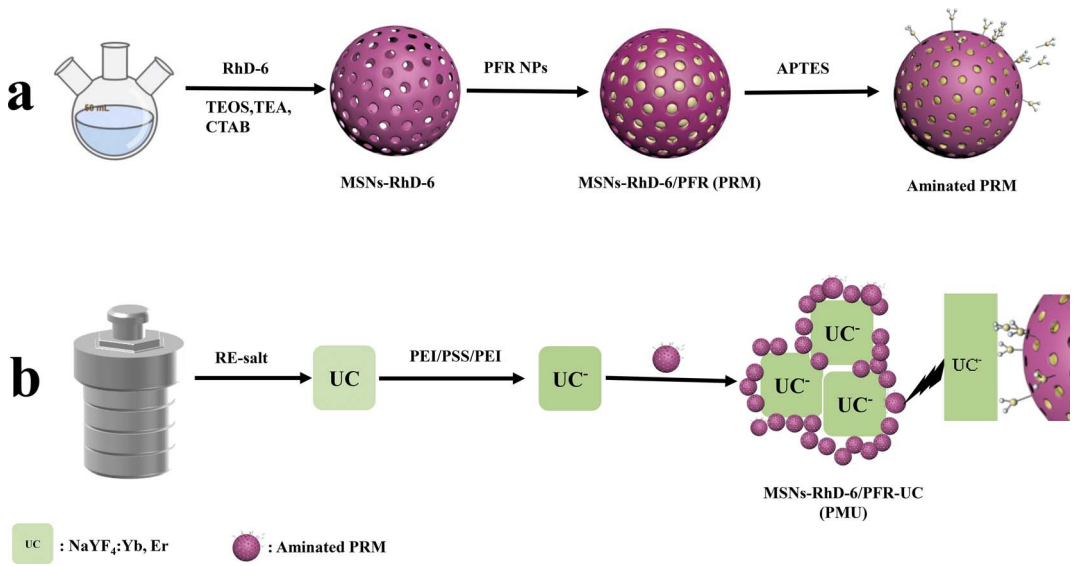

Scheme 1 The illustration of preparation of PRM (a), UC and PMU (b) composites.

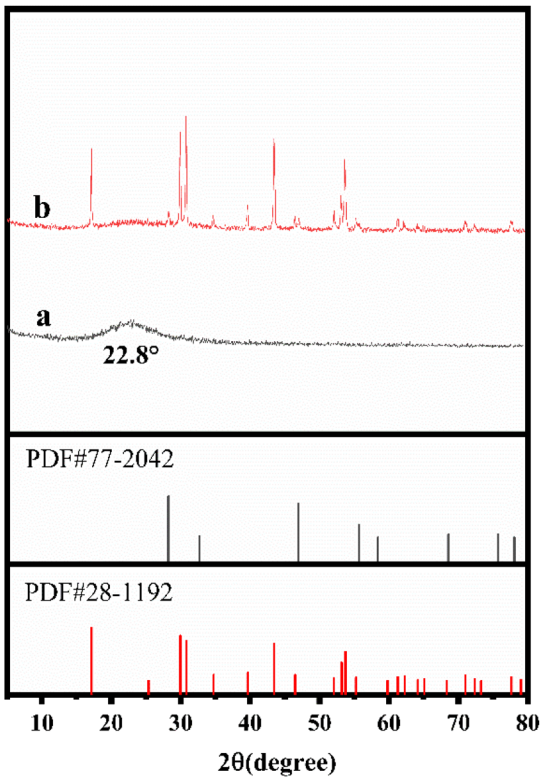

Fig. 1 X-ray diffraction patterns (a) RPM, (b) PMU.

vibration of the silicone hydroxyl O–H groups on the surface of the material. The absorption peaks appearing at 1100 and 800 cm^{-1} are due to the bending vibration of the symmetric Si–O–Si and the asymmetric stretching. The peaks at 2926 and 2855 cm^{-1} may be related to the C–H stretching vibrations of the small amount of CTAB present in the MSNs NPs. In addition, there is a very significant fluctuation in the absorption between 1600 and 800 cm^{-1}, which is mainly due to the presence of Cl-PFR, and the above proves the successful synthesis of PRM. No obvious change can be observed for PMU in Fig. 2b, line b, although UC nanoparticles were coated on it.

The morphology of PMU (Fig. 3a) and RPM (Fig. 3b) were characterized by TEM. As shown in Fig. 2, the as-synthesized RPM particles are porous with a size of about 40 nm, indicating that RPM has a large specific area and strong adhesive. After mixing RPM with UC nanoparticles, the compounds became aggregated due to their electrostatic adsorption of them. The elemental mapping of the as-synthesized PMU (Fig. 3d–g) has been measured, and the elemental of Si, O is uniformly distributed on the PRM nanosphere part. While Y and F are UC parts, the results are in good agreement with the XRD spectra. However, the PFR NPs is too small to observed with the TEM in the composites.

3.2 The fluorescence property of the as-synthesized FRET composites

To demonstrate the PMUs with FRET effect and dual-channel characteristics, the up/down conversion fluorescence spectra were measured. As shown in Fig. 4a, PFR NPs have a significantly broad emission band at 536 nm (line a), and MSNs-RhD-6 nanospheres are optimally excited spectra near 528 nm (line b), where their emission and absorption bands mostly overlap. According to the FRET rule, when the distance between PFR NPs and MSNs-RhD-6 is near 10 nm, the PFR NPs can act as donors and transfer energy to MSNs-RhD-6 (acceptor), then the fluorescence intensity at 560 nm becomes strong.[30] Fig. 4b shows the increased fluorescence intensity of the PFR NPs coupled MSNs-RhD-6 composites at 560 nm than pure MSNs-RhD-6 (line c) with the increased PFR NPs amount in the composites from 0.1 to 0.2 mg mL^{-1} (line a and line b), while the fluorescence intensity at 528 nm decreased with the increased PFR amount in the composites. It is a good demonstration of the FRET between PFR NPs and MSNs-RhD-6. However, the fluorescence intensity decreased obviously once the concentration of PFR was over 0.2 mg mL^{-1} (line d). Thus, the 0.2 mg mL^{-1} PFR NPs in the composites were used in this experiment. To introduce the up-conversion luminescence mechanism, the UC NPs were used as carriers to construct the PMU composites. As shown in Fig. 4c, the fluorescence intensity of the PMU increased with the increased UC NPs, with the amount ratio between UC and RPM

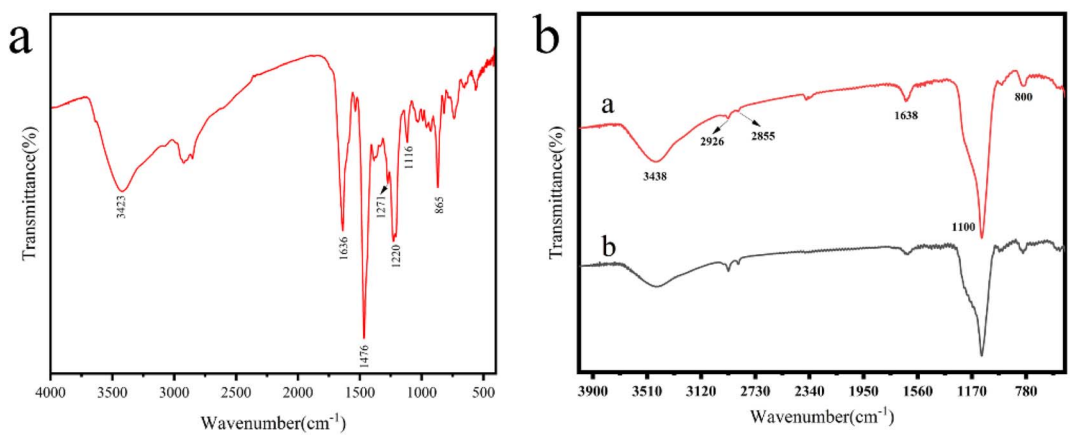

Fig. 2 Fourier transform infrared spectra (FTIR) of (a) Cl-PFR, (b) PRM (line a), PMU (line b).

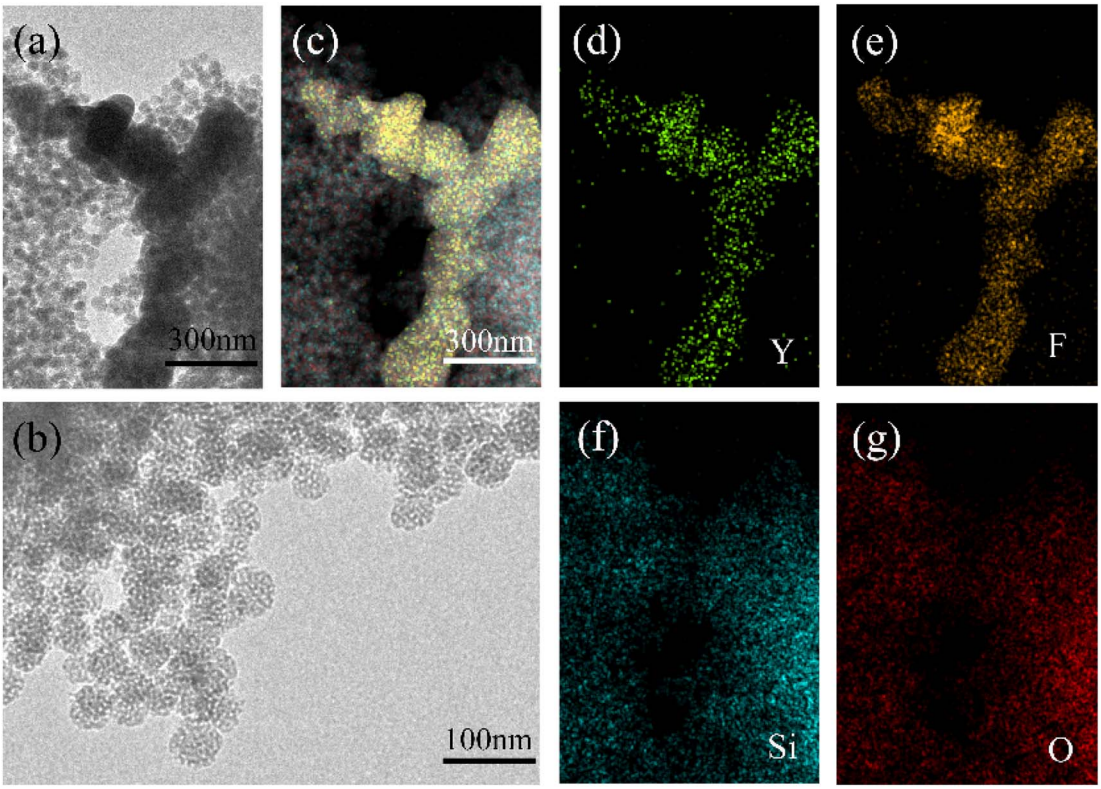

Fig. 3 TEM images of PMU (a), PRM (b) and the element mapping maps of PMU (c–g).

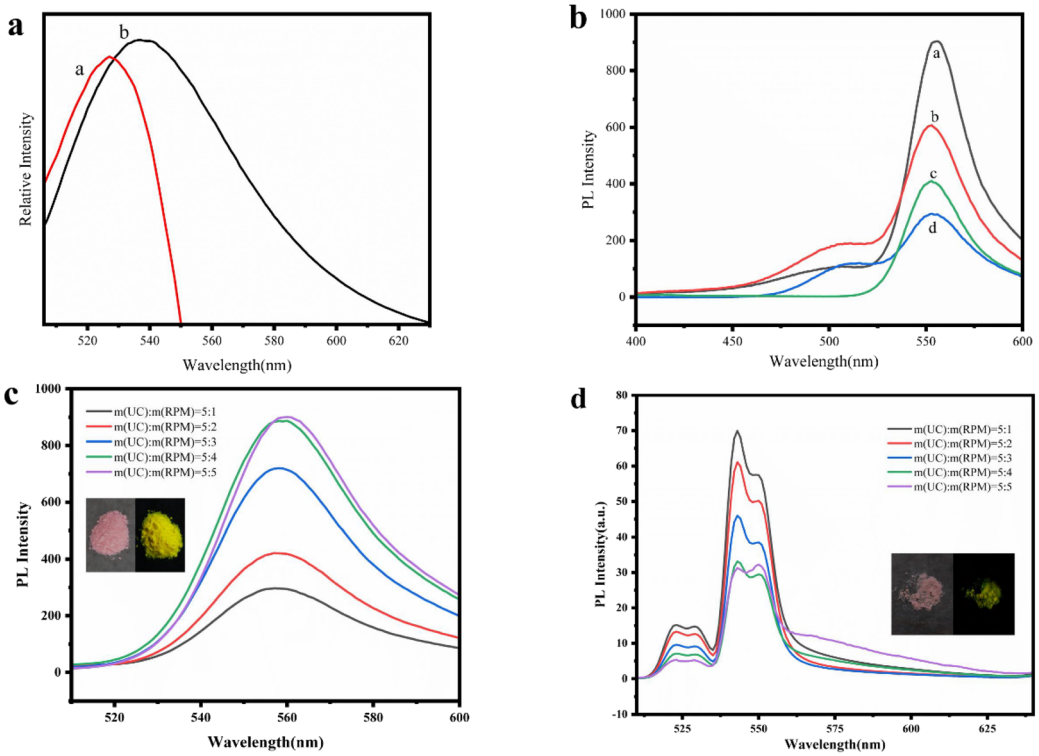

Fig. 4 (a) The emission peaks of PFR NPs (curve a) and the excitation peaks of MSNs-RhD-6 (curve b); (b) the PL of FRET probes composed of different concentrations of PFR NPs spectra (a, 0.2; b, 0.1; c, 0; d, 1 mg mL^{-1}) and MSNs-RhD-6; (c and d) emission spectra of PMU at different mass ratios of UC and PRM.

from 5 : 1 to 5 : 4 in the composites. However, the fluorescence intensity didn't increase obviously at the amount ratio of 5 : 5. Fig. 4d shows that the fluorescence intensity of PMU decreased with the increased amount ratio UC and RPM under the irradiation of 980 laser. To balance the fluorescence intensity of composites under the irradiation of UV and 980 light, the amount ratio of 5 : 2 of UC and RPM was used.

3.3 The application of the as-synthesized FRET composites in the LFPs

Prior to the development of LFP detection using PMU composites, the composites were subjected to grinding and removal of large particles using a 200 mesh sieve. The PMU powder was then applied to the LFP detection using a feather brush, and the excess powder was removed using an ear wash ball to prevent damage to the LFPs. The surface of the substrate can be categorized as perforated or non-perforated based on its flatness.[6] Examples of perforated surfaces include A4 paper and marble blocks, while non-perforated surfaces mainly include glass, plastic boxes, metal, and tiles. To investigate the effects of porosity of the as-synthesized PMU nanocomposites, we chose a variety of common items made from porous and non-porous materials, such as glass, iron sheets, marble blocks, locks, A4 paper, courier bags, blue plastic boxes, and shockers.

When powder dusting the as-synthesized composites onto the LFPs with various substrate surfaces, the images were displayed through irradiation with 365 nm UV light and 980 nm laser under the same conditions. As shown in Fig. 5a–h, the clarity and contrast of the LFPs have varied greatly due to the affection of the color, pattern and flatness of the substrate when displayed in natural light. The fingerprints treated with the as-synthesized PMU on glass, courier bags, locks and blue plastic boxes can be observed. However, the fingerprints on the A4 paper and oscillator housing can not be distinguished. Fig. 5a'–h' shows the fingerprints on the substrates under the irradiation of 365 nm UV light, which demonstrated that the fingerprints on the substrates of glass, iron sheets, express bags, marble, and lock could be distinguished clearly, but the effect of background fluorescence of the substrate causes the images of the fingerprints to be invisible on A4 paper, blue plastic box and oscillator housing. Compared to the images observed under daylight and 365 nm UV light, the fingerprints observed with the irradiation of 980 nm laser (Fig. 5a"–h") are clearer. Moreover, the fingerprints on the substates of the blue plastic box, A4 paper, and oscillator housing can be observed to be distinguished, which can effectively avoid the interference of the background fluorescence of the substrate under 365 nm UV light irradiation, making the use of material development broader and more sensitive. The result displays that the PMU composite can effectively avoid background interference and significantly improve the accuracy of LFP development.

Furthermore, the details of fingerprint development are often divided into 3 levels. The details of the first level (level 1) contain shapes such as nuclei, triangles, and arches; the details of the second level (level 2) are for macroscopic features of ridge grooves such as finger bifurcations, terminations, islands, and short ridges; the details of the third level (level 3) defines microscopic features of ridge grooves with sweat holes, ridge paths, and edge contours.[5,6,32] In general, level 1 features are not obvious, while level 2 and 3 fine features are obvious and are more suitable and valuable for fingerprint identification.[33–36] Fingerprint details under 980 nm infrared light are shown in Fig. 6; all fingerprints show clear localized features such as nuclei, triangles and loops. Fingerprint details such as bifurcations, terminations, breakpoints, hooks, islands, short ridges and sweat pores are enhanced when the photo is appropriately

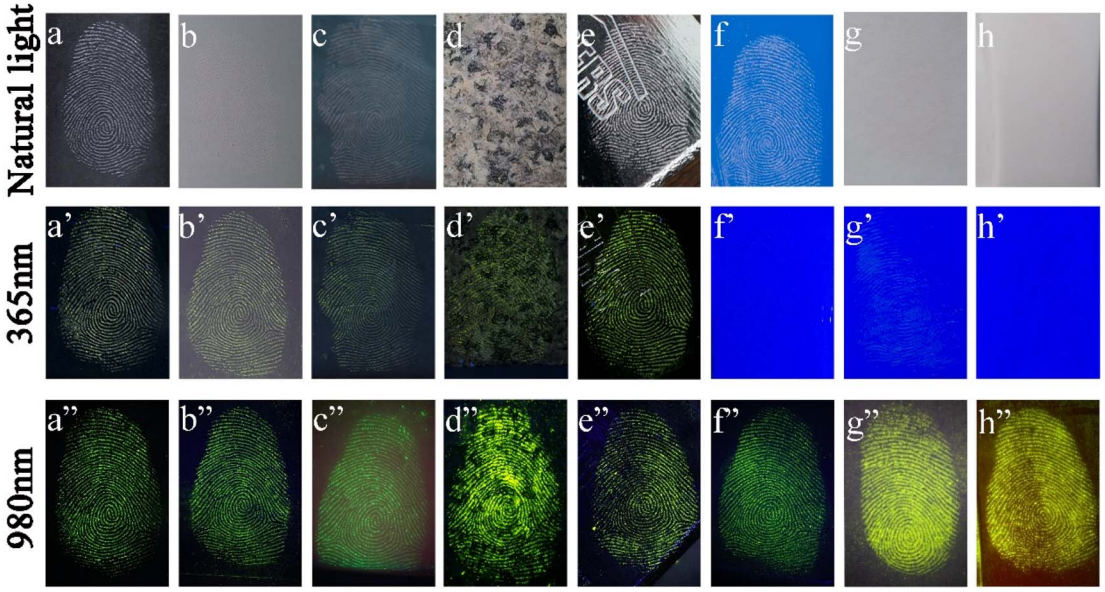

Fig. 5 LFPs fluorescence images of different substrates under natural light (a–h), 365 nm UV light (a'–h') and 980 nm laser (a"–h"). Substrates: (a, a' and a") glass, (b, b' and b") iron sheets, (c, c' and c") express bags, (d, d' and d") marble, (e, e' and e") lock, (f, f' and f") blue plastic box, (g, g' and g") A4 paper, (g, g' and g") (h, h' and h") oscillator housing.

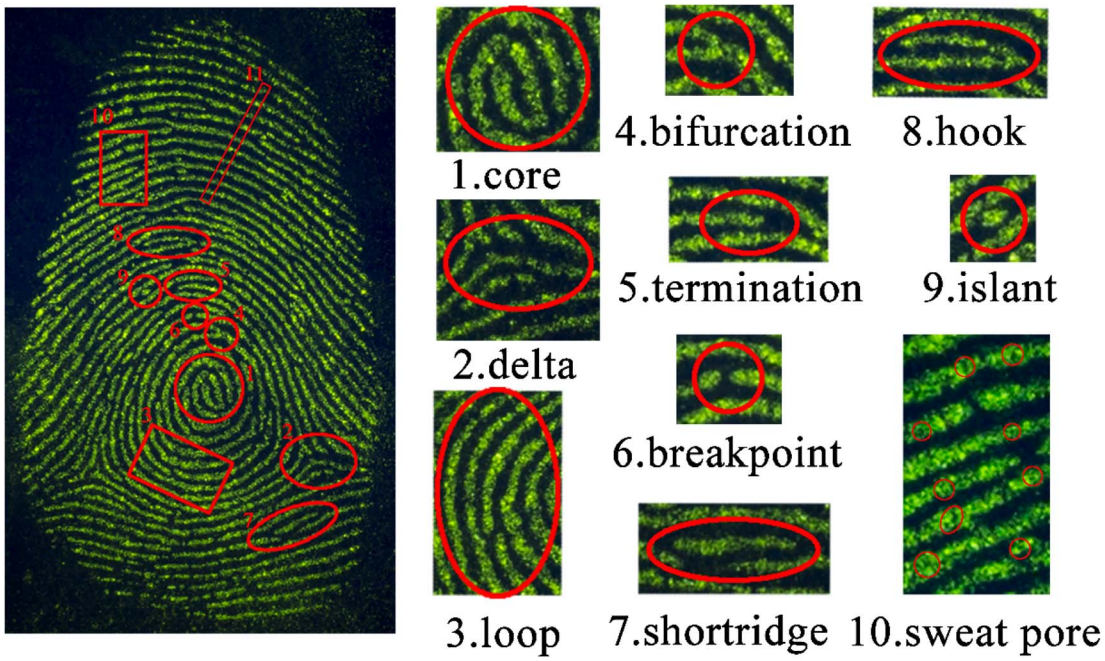

Fig. 6 Specific details of fingerprints on glass of PMU composite under 980 nm laser. Including (1) nucleus, (2) triangle, (3) ring *etc.*, (4) bifurcation, (5) termination, (6) break point, (7) short ridge, (8) hook, (9) island and (10) sweat hole.

enlarged. Fig. 7 shows the periodic variation of luminescence intensity between the ridge and groove in Region 11 of Fig. 6.

Various complex conditions may be encountered at the crime scene, especially after rainwater flushing and old LFPs. The effect of the rain was mimicked by rinsing the LFPs with a water tap, and Fig. 8a–c shows the LFPs development effects after 10 minutes and 30 minutes of rinsing, respectively. It can be seen that the fingerprint photos after different rinsing times still have good legibility and the fingerprint details are clearly discernible. As shown in Fig. 8a'–e', PMU was gently applied to detect fingerprints on the glass using a feather brush and aged for 1 day, 2 days, 3 days, 5 days, 7 days and up to 15 days for development. The details of fingerprints aged 1–7 days were very clear and the contrast of fluorescence did not change much. After 15 days of storage, the fingerprint details were still clearly recognizable, although the fluorescence intensity of the

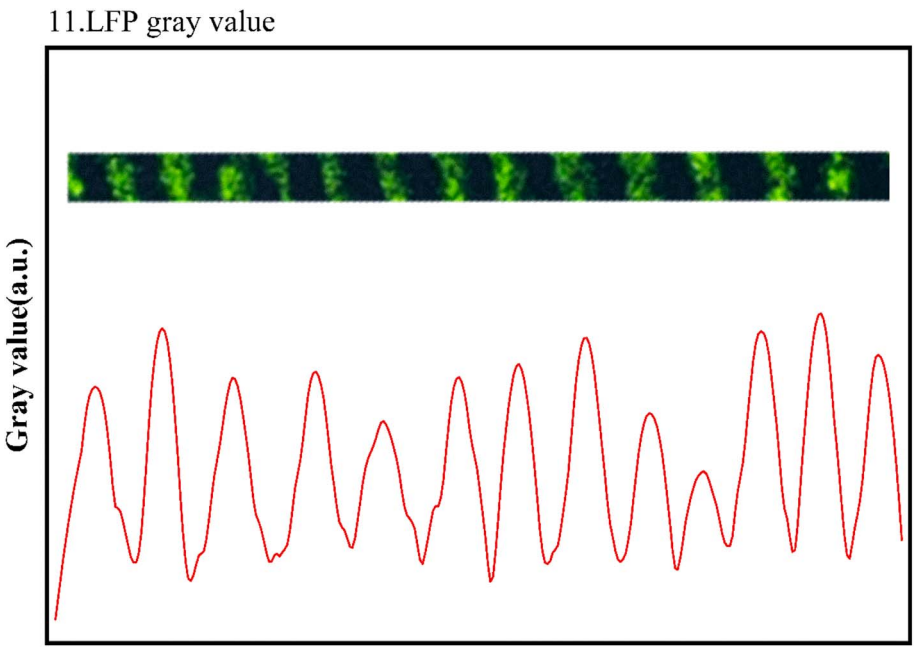

Fig. 7 Grayscale values of LFP.

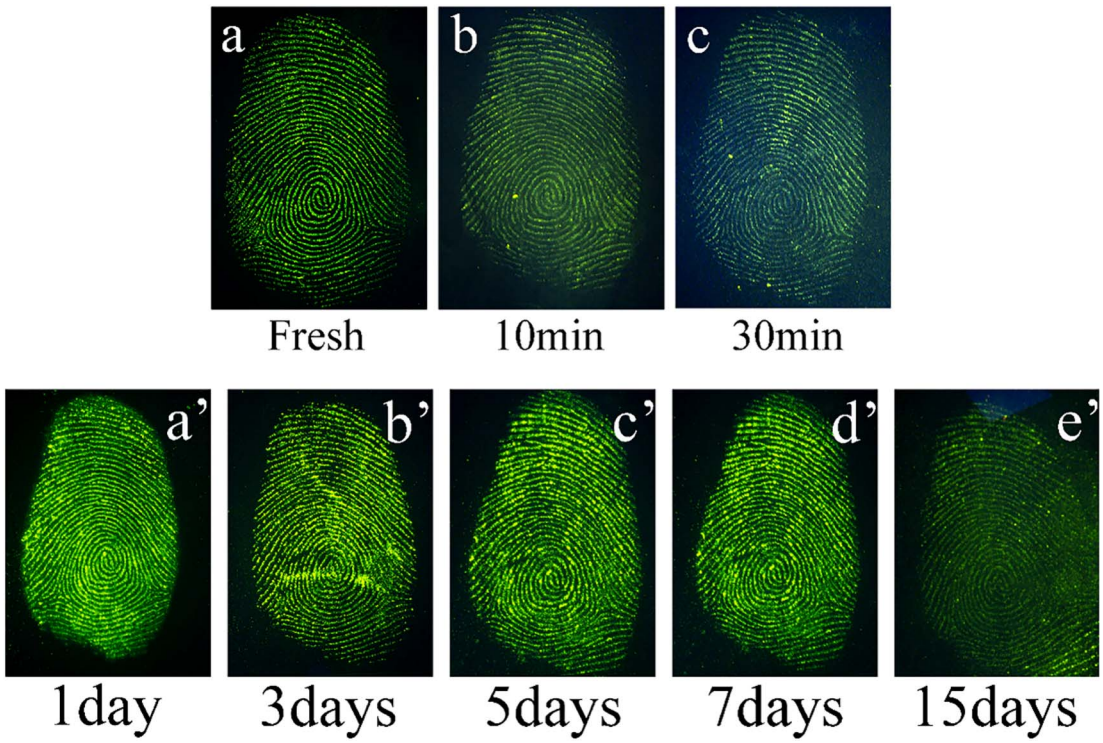

Fig. 8 The rinse (a, fresh LFP without rinse; b, 10 min rinse; c, 30 min rinse) and aging (a', 1 day; b', 2 days; c', 3 days; d', 4 days; e', 15 days) effect of the LPSs in the presence of the as-synthesized PMU composite under the irradiation of 980 nm laser.

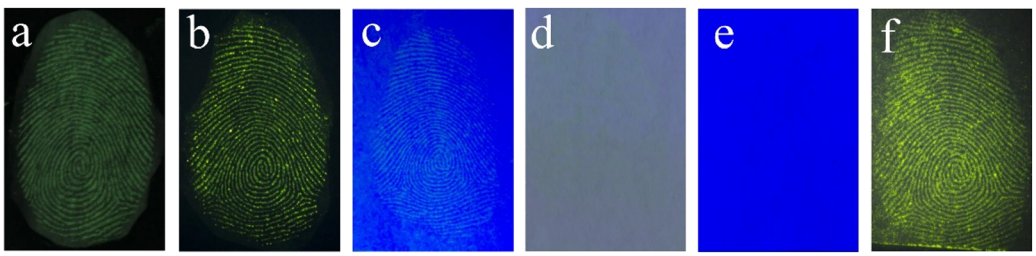

Fig. 9 Latent fingerprint images on glass developed with commercially available established products (a) and on synthesized PMU composites (b) under 365 nm UV irradiation; latent fingerprint images on paper developed with commercially available established products (c, 365 nm UV irradiation; d, 980 nm laser irradiation) and on synthesized PMU composites (e, 365 nm UV irradiation; f, 980 nm laser irradiation).

fingerprints became diminished. This decreased intensity may be caused by losing substances in the fingerprint over time. Typically, fingerprints exposed to rain and aging lose moisture, lipids, and other components, which can make fingerprint visualization more difficult. Nevertheless, our synthesized PMU composites maintained good readability and clarity, which suggests that the PMU composites have excellent adsorption capacity and fluorescence stability.

A comparison was made between the as-synthesized PMU composites and established products available on the market to assess the effectiveness of detecting latent fingerprints on glass and paper. Results depicted in Fig. 9a revealed that existing products in the market performed well in developing fingerprints on glass under 365 nm UV light. Similarly, the as-synthesized PMU composites exhibited comparable results on glass under the same UV irradiation conditions (Fig. 9b). However, when examining fingerprint development on paper, the market products displayed poor results under both 365 nm UV light (Fig. 9c) and 980 nm laser (Fig. 9d) irradiation. Despite the subpar performance of synthesized PMU composites in developing fingerprints on paper under 365 nm UV light, clear fingerprint images can be observed under 980 nm laser irradiation (Fig. 9e and f). The result indicates that the as-synthesized PMU composites hold promise for fingerprint development applications due to their dual-channel property.

4. Conclusion

A novel PMU fluorescent material that utilizes the FRET effect and reversible dual-channel properties was developed to improve the sensitivity and contrast of fingerprint detection under different conditions. Under 365 nm UV and 980 nm laser

irradiation, the details of fingerprints can still be clearly revealed even when they are aged or washed. Using a 980 nm laser for the LFPs detection avoids background interference and shows high contrast and accuracy for complex scenes. Compared with commercially available products, PMU composites have better developing effects and applicability, which predicts a wide range of applications in the field of latent fingerprint detection.

Conflicts of interest

There are no conflicts to declare.

Acknowledgements

This work was supported by the Anhui Province Natural Science Foundation Project (2308085MB52), the Key Research and Development Projects of Anhui Province (202104d07020013); the launching scientific research funds for doctors of Anhui University of Science and Technology (11109).

References

1 A. A. Ansari, K. M. Aldajani, A. N. Alhazaa and H. A. Albrithen, *Coord. Chem. Rev.*, 2022, **462**, 214523.
2 D. Chávez, C. R. Garcia, J. Oliva and L. A. Diaz-Torres, *Ceram. Int.*, 2021, **47**, 10.
3 N. Singla, M. Kaur and S. Sofat, *Forensic Sci. Int.*, 2020, **309**, 110187.
4 X. Liu, X. J. Su, Z. H. Ren, L. Q. Yang, X. Y. Zhang and M. Y. Ding, *Spectrochim. Acta, Part A*, 2024, **305**, 15.
5 K. Song, P. Huang, C. L. Yi, B. Ning, S. Hu, L. M. Nie, X. Y. Chen and Z. H. Nie, *ACS Nano*, 2015, **9**, 12344.
6 K. X. Yang, H. J. Tang, Y. X. Jiao, L. Gao, M. F. Zhang, J. Qin, W. Y. Li, S. Y. Lu and Y. H. He, *J. Lumin.*, 2023, **25**, 119721.
7 M. Saif, N. Alsayed, A. Mbarek, M. El-Kemary and M. S. A. Abdel-Mottaleb, *J. Mol. Struct.*, 2016, **1125**, 763.
8 Y. J. Kim, H. S. Jung, J. Lim, S. J. Ryu and J. K. Lee, *Langmuir*, 2016, **32**, 8077.
9 G. S. Sodhi and J. Kaur, *Forensic Sci. Int.*, 2001, **120**, 172.
10 T. Wei, J. C. Han, L. Wang, J. Q. Tao, H. Zhang, D. Xu, S. J. Su, C. Fan, W. G. Bi and C. Sun, *Nanoscale*, 2021, **13**, 12038.
11 O. P. Jasuja, A. Kaur and P. Kumar, *Forensic Sci. Int.*, 2012, **223**, 47.
12 S. Oden and B. Von Hofsten, *Nature*, 1954, **173**, 449.
13 G. S. Sodhi and J. Kaur, *Egypt. J. Forensic Sci.*, 2016, **6**, 44.
14 S. Shahbazi, R. Boseley, B. Grant, D. Chen, T. Becker, O. Adegoke, N. Nic Daéid, G. Jia and S. W. Lewis, *Forensic Chem.*, 2020, **18**, 100222.
15 S. Chatterjee, X. S. Li, F. Liang and Y. W. Yang, *Small*, 2019, **15**, 1904569.
16 K. Malhotra, D. Hrovat, B. Kumar, G. C. Qu, J. Van Houten, R. Ahmed, P. a. E. Piunno, P. T. Gunning and U. J. Krull, *ACS Appl. Mater. Interfaces*, 2023, **2**, 2499.
17 J. Wang, T. Wei, X. Y. Li, B. H. Zhang, J. X. Wang, C. Huang and Q. Yuan, *Angew. Chem., Int. Ed.*, 2014, **53**, 1616.
18 S. G. Wang and L. Y. Wang, *TrAC, Trends Anal. Chem.*, 2014, **62**, 123.
19 M. Wang, D. Shen, Z. Zhu, J. Ju, J. Wu, Y. Zhu, M. Li, C. Yuan and C. Mao, *Mater. Today Adv.*, 2020, **8**, 100113.
20 M. Wang, M. Li, M. Y. Yang, X. M. Zhang, A. Y. Yu, Y. Zhu, P. H. Qiu and C. B. Mao, *Nano Res.*, 2015, **8**, 1800.
21 H. Shao, F. Li, D. Li, Q. L. Ma, W. S. Yu, G. X. Liu and X. T. Dong, *ACS Appl. Nano Mater.*, 2022, **5**, 3333.
22 A. Baride, G. Sigdel, W. M. Cross, J. J. Kellar and P. S. May, *ACS Appl. Nano Mater.*, 2019, **2**, 4518.
23 L. Tang and J. J. Cheng, *Nano Today*, 2013, **8**, 290.
24 X. Y. Qiu, S. H. Han, Y. F. Hu, M. Gao and H. Wang, *J. Mater. Chem. A*, 2014, **2**, 1493.
25 J. Sha, Y. Song, B. Liu and C. Lü, *Microporous Mesoporous Mater.*, 2015, **218**, 137.
26 L. J. Wang, W. H. Gu, Z. B. An and Q. Y. Cai, *Sens. Actuators, B*, 2018, **266**, 19.
27 P. Yang, W. Sun, Z. K. Zhang and H. L. Xing, *Luminescence*, 2022, **37**, 1873.
28 P. Yang, Y. Zhao, Y. Lu, Q. Z. Xu, X. W. Xu, L. Dong and S. H. Yu, *ACS Nano*, 2011, **5**, 2147.
29 S. Zadran, S. Standley, K. Wong, E. Otiniano, A. Amighi and M. Baudry, *Appl. Microbiol. Biotechnol.*, 2012, **96**, 895.
30 S. R. Guo, J. Y. Gong, P. Jiang, M. Wu, Y. Lu and S. H. Yu, *Adv. Funct. Mater.*, 2008, **18**, 872.
31 J. Kobler, K. Möller and T. Bein, *ACS Nano*, 2008, **2**, 791.
32 P. Singh and S. Kumar, *ChemistrySelect*, 2023, **8**, 29.
33 S. Hohng, S. Lee, J. Lee and M. H. Jo, *Chem. Soc. Rev.*, 2014, **43**, 1007.
34 Y. Q. Wang, J. Wang, Q. Q. Ma, Z. H. Li and Q. Yuan, *Nano Res.*, 2018, **11**, 5499.
35 V. Sharma, S. Choudhary, P. Mankotia, A. Kumari, K. Sharma, R. Sehgal and V. Kumar, *TrAC, Trends Anal. Chem.*, 2021, **143**, 116378.
36 E. Prabakaran and K. Pillay, *J. Mater. Res. Technol.*, 2021, **12**, 1856.